Characterization of morphology transitions in diffusion-controlled systems

E. Ben-Jacob and P. Garik

Department of Physics, Randall Laboratory, University of Michigan, Ann Arbor, Michigan 48109
and Department of Condensed Matter Physics, School of Physics and Astronomy, Tel Aviv University, 69978 Tel Aviv, Israel

T. Mueller and D. Grier

Department of Physics, Randall Laboratory, University of Michigan, Ann Arbor, Michigan 48109

We provide a theoretical and experimental study of the nature of morphology transitions in diffusion-controlled systems. The interplay of surface tension and kinetic anisotropy is found to determine the selected morphology in an anisotropic Hele-Shaw cell experiment, and in theoretical computations in the boundary-layer model (BLM) for solidification. We employ the Hele-Shaw cell to demonstrate the existence of surface tension and kinetic dendrites. Using the BLM we show that the selected velocities for kinetic and surface-tension dendrites scale differently with the undercooling Δ. A study of the selected velocity as a function of undercooling is presented for both aligned and competing anisotropies, the latter motivated by the Hele-Shaw experiment. The difference in scaling is related to the reentrant tip splitting found for the case of competing anisotropies in the BLM morphology diagram via a time-dependent solution for the interface evolution. We suggest that the nature of the transitions between morphologies should be classified by the behavior of the selected interfacial velocity as a function of driving force. For the case of the BLM, first- and second-order-like morphology transitions, by analogy to phase transitions, are discussed. We further advance the hypothesis that the fastest growing morphology, whether it be tip splitting or dendritic, emerges as the stable interfacial morphology experimentally. We support our hypotheses by drawing analogies to experimental results of growth from supersaturated solutions and by electrochemical deposition.

INTRODUCTION

Over the past several years unifying principles governing the development of interfacial patterns have been arrived at. It is now recognized that structures whose growth is diffusion-controlled share a common set of interfacial patterns with qualitative rules of morphology correspondence between systems which can be established by careful identification of the control parameters. For a given system these results are well summarized in a morphology diagram delineating the selected morphology as a function of the control parameters.[1-4] Part of the beauty of this field has been the success of simple theoretical models and experimental systems in exposing the underlying physics. For example, the discovery that microscopic anisotropy in either the dynamics of surface tension or kinetic growth is a singular perturbative control necessary to stabilize dendritic growth, was first achieved in the boundary-layer model for solidification[5] (BLM), and the geometrical model.[6] This further led to the resolution of the problem of the selected velocity of the needle crystal.[7,8] It is also the prediction of these models that in systems with weak effective anisotropy tip-splitting growth occurs which can be identified with the dense branching morphology[9] (DBM). Although some of these results have now been achieved for the full nonlocal diffusion problem,[10-13] the local models retain the appeal of capturing the correct fundamental physics while remaining computationally tractable for the time evolu-

tion of the interface. Similarly, the simple experiment of Hele-Shaw viscous fluid displacement[1,4,14-17] has proved a lucid method to demonstrate the effects of anisotropy, and provides an important means to develop intuition as to the dominant effects in morphology determination.

In this paper we focus on morphology selection and the nature of the transition between morphologies as diffusion-controlled systems pass from near-equilibrium to far-from-equilibrium dynamics. We first present the results of experiments in an anisotropic Hele-Shaw cell where the presence of competing surface-tension and kinetic anisotropies[1,4] allows the clear distinction to be made between dendrites stabilized by surface-tension anisotropy for small applied pressure, and dendrites stabilized by kinetic effects at larger pressure. This motivates our study of morphology transitions in the BLM where we find that *the velocity of the selected needle crystal scales differently with undercooling in the surface tension and kinetic anisotropy regimes.* Specifically, for intermediate undercoolings of $0.2 < \Delta < 0.6$ the selected velocity V^* scales roughly as Δ^5 for surface-tension needle crystals, while for kinetic needle crystals V^* goes roughly as Δ^8. This difference in scaling correlates well with the observation of reentrant tip splitting in our Hele-Shaw experiment. This tip-splitting growth (presumably the DBM) is observed between the regimes of surface-tension and kinetic dendrites. As explained below, it arises naturally for anisotropic Hele-Shaw interface development because surface-tension and kinetic effects are in competing

directions. This observation motivated our study of BLM simulations with the introduction of an offset angle between the surface-tension and kinetic anisotropies. For parameters chosen such that the two different anisotropies are of roughly equal "strengths" (as judged by the equality of the surface tension and kinetic selected velocities), just such reentrant tip splitting is also observed in the BLM.

To develop a quantitative characterization of such morphology transitions we propose below that a natural scheme of a morphology diagram is one with axes of interfacial velocity versus driving force. The example we study is that of the selected needle-crystal velocity V^* as a function of undercooling for the BLM. We find that for the BLM a plot of V^* versus Δ can display discontinuities or sudden changes in slope corresponding to changes in the selected morphology. By analogy to phase transition terminology we dub these first- and second-order-like morphology transitions, respectively. An examination of the so-called "mismatch" function which determines the selected velocity shows that it may fail to vanish when the morphology transition is first-order-like. In addition, our numerical study of the BLM needle crystal shows that in the presence of competing surface-tension and kinetic anisotropy it is possible for there to be more than one selected needle crystal. By studying the time-dependent evolution of the slower one we show that it is unstable and undergoes tip splitting. This motivates our hypothesis that just as it is the fastest growing needle crystal which is the stable and selected one when there is no such competition, so more generally it is the fastest growing morphology which is selected. We extend this argument to the regime where we believe tip splitting should dominate the interfacial growth.

Finally, we support our new characterization of morphology transitions by making comparison to the earlier results of Chan et al.[18] and the results of electrochemical deposition experiments. Although the physical mechanisms underlying morphology transitions in real experimental systems are likely not identical in nature to the competing anisotropies BLM model we have solved, nevertheless in these experimental systems when the velocity is plotted against the driving force changes in slope and discontinuities correspond to changes in the observed morphology.

MORPHOLOGY DIAGRAM FOR ANISOTROPIC HELE-SHAW FLOW

In this section we study interfacial development as determined by surface-tension and kinetic effects in a Hele-Shaw system with both surface-tension and kinetic anisotropies. Moreover, in the experiment described below the anisotropies are in competing directions resulting in the particularly rich morphology diagram of Fig. 1. Our key finding is that such competitive anisotropies permit a morphology regime of tip splitting, which is probably dense-branching growth, between dendrites which are stabilized alternately by surface tension anisotropy and kinetic anisotropy.

The anisotropic Hele-Shaw experiments were performed in the same cell as described by Ben-Jacob et al.[1]
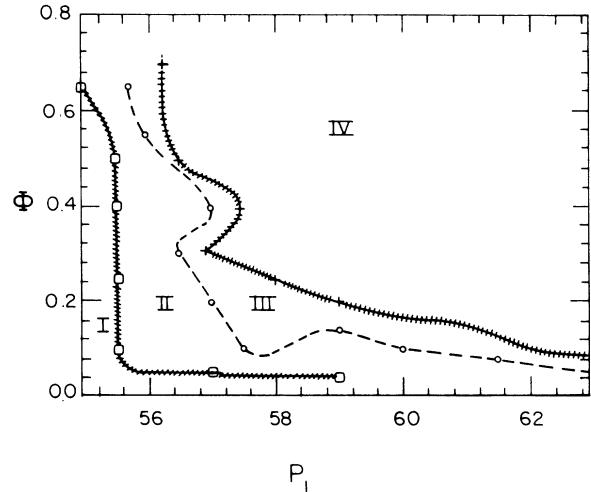

FIG. 1. Morphology diagram for a sixfold anisotropic Hele-Shaw cell. Here P_1 is the applied pressure measured roughly in centimeters of Hg (the actual manometer fluid was a light oil). The anisotropy of the cell is measured by the ratio $\Phi = b_1 /(b_0 + b_1)$ where b_1 is the depth of the grooves (0.015 in) and b_0 is the additional spacing between the top plate and the top of the grooved plate The morphology regions are I, faceted growth; II, surface-tension dendritic growth; III, tip-splitting growth; IV, kinetic dendritic growth. Cross hatching of curves separating labeled morphology regions indicates possible existence of narrow regions of other morphologies, e.g., as mentioned in the text between regions I and II there is evidence for DBM growth.

To review the experimental apparatus, air was pumped into glycerol which was used again as the viscous fluid. High purity glycerol (94%) dyed with food color was used. On the circular bottom plate, radius $R_0 = 25$ cm, was ruled a regular sixfold lattice of grooves with depth $b_1 = 0.015$ in and width of 0.03 in. The effective anisotropy of the system, defined by $\Phi = b_1 /(b_0 + b_1)$, was varied by changing the spacing b_0 between the cell plates. The range for Φ in the experiments was between 0.1 and 1.0. Pressures ranging up to 100 mm Hg were applied from a large (≈ 5 gal) pressure reservoir.

The classification of the morphologies was made at the time when the average interfacial radius R was half the radius of the circular plate R_0. Specification of the radius at the point of classification is necessary since the pressure field in the glycerol satisfies the Laplace equation $\nabla^2 p = 0$. Thus, the effective driving force, proportional to $(p_{\text{applied}} - p_{\text{atm}})/R \log(R/R_0)$, increases with R with a consequent possible variation of morphology with time. In practice, this did not prove a problem in morphology identification. The morphologies observed, as a function of increasing applied pressure at a fixed effective anisotropy, are as follows.

At the lowest pressures applied faceted growth occurred [Fig. 2(a)]. Flat interfaces that advanced a row at a time via nucleation and subsequent kink propagation were observed. At slightly larger pressures both the nucleation time and the time for the propagation of a kink along the entire length of a facet becomes shorter, but

with the nucleation time shorter than the propagation time. As a result, each face develops multiple propagating kinks. The upshot is an interface smooth on the scale of the interchannel spacing due to the overlap of the multiple kinks. However, the row by row advance is also sufficiently disturbed to produce roughness on a multiple channel scale. Characterization of this dynamic morphology requires a larger system. In this regime, between faceted and dendritic growth, tip splitting is observed.

As the applied pressure is further increased the first transition to dendritic growth occurs. The underlying needle crystals point at a 30° angle to the direction of the lattice grooves [Fig. 2(b)]. For reasons to be explained below, we designate these as surface-tension anisotropy dendrites. With a continued increase of pressure the selected morphology once again becomes tip splitting
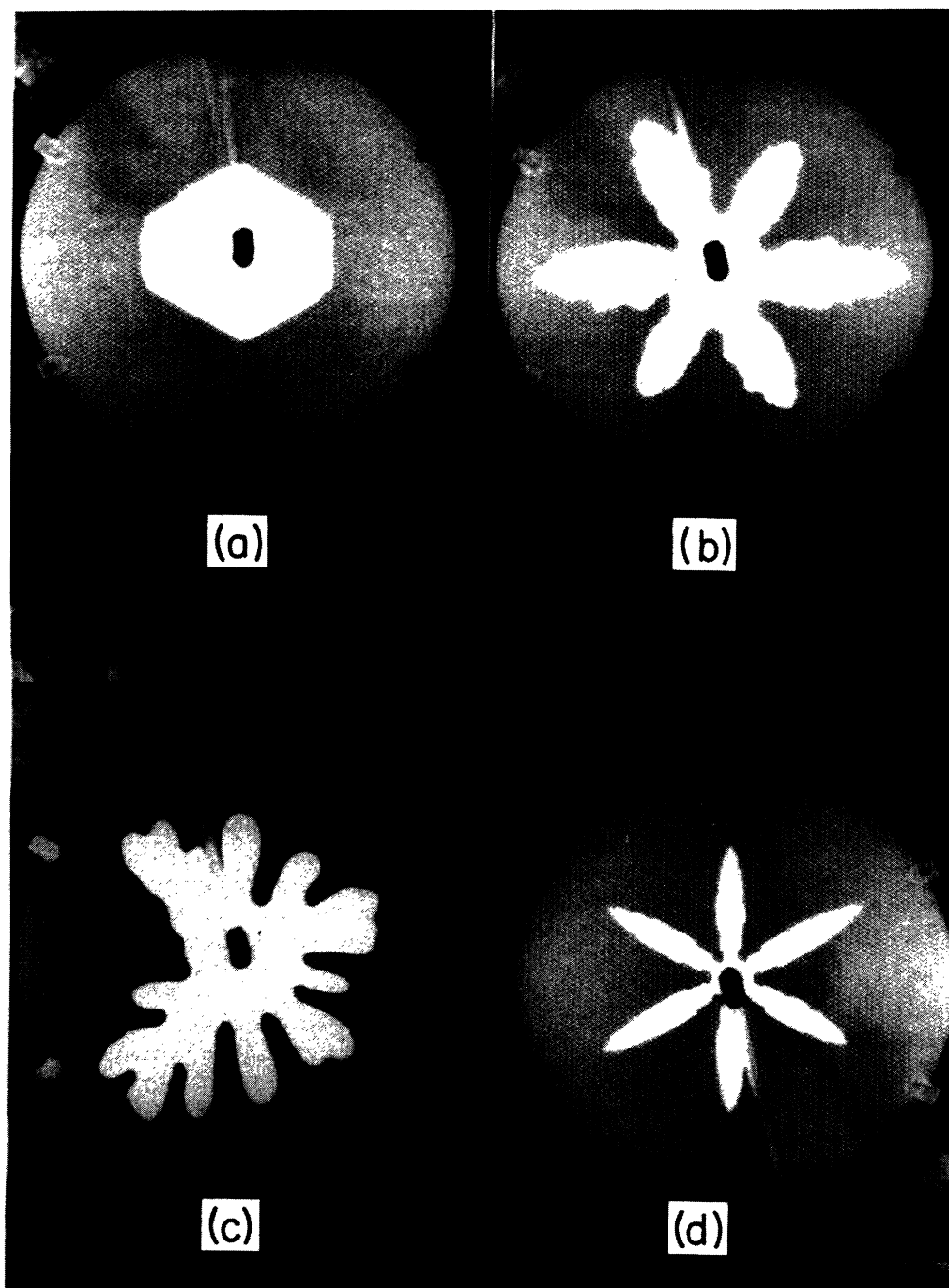

FIG. 2. Morphologies corresponding to the morphology diagram in the anisotropic Hele-Shaw cell. (a) Faceted growth. (b) Surface-tension dendrites. With careful inspection it is possible to observe that the dendrite tips are pointed at an angle of 30° to the ruling of the grooves. (c) Tip-splitting growth. In a larger and more regular cell we assume that this would be a dense-branching growth. (d) Kinetic dendrites. The needle crystals grow parallel to the ruled channels.

[Fig. 2(c)]. Presumably this is the DBM; however, relative to the dimensions of this small cell the typical branch width is too large to produce the multiple tip splitting necessary for a clear-cut identification. (On the other hand, in a demonstration cell with smaller interchannel spacing than in the experimental cell desired above, it was possible to plainly identify a range of DBM growth after the surface-tension dendrite regime.) Finally, at high driving force sixfold dendritic growth aligned with the channels occurs [Fig. 2(d)]. These we refer to as kinetic dendrites. Between the DBM and kinetic dendrite regimes is a region in which the morphology is that of needle crystals without side branches. Within the resolution of our measurements (pressure steps of 5–10 mm Hg) the transition to needles from either the DBM or kinetic dendrite sides is sharp. Nevertheless, at present we identify kinetic dendrites and undecorated needle-crystal growth as the same morphology.

A qualitative understanding of the morphology diagram can be arrived at by considering the interfacial boundary condition and the velocity field of the Hele-Shaw cell. Thus, the pressure at the interface p_s and the velocity normal to the interface v_n are determined from

$$p_s = p_1 - d(\theta)\kappa - \beta(\theta)v_n \ , \tag{1}$$

$$v_n = \frac{-b(\theta)^2}{12\eta}\nabla p \cdot \hat{n} \ , \tag{2}$$

where κ is the local curvature of the interface, η is the viscosity of the glycerol, and $\hat{n}$ is a unit normal to the interface. Moreover, the dependence of the interfacial surface-tension and kinetic term vary with the plate spacing in the Hele-Shaw cell. For the anisotropic cell this variation on plate spacing $b(\theta)$ gives rise to the angular dependence of the surface tension $d(\theta)$, and the kinetic factor $\beta(\theta)$.

It is the resultant angle-dependent competition between the terms $d(\theta)\kappa$ and $\beta(\theta)v$ which gives rise to distinct kinetic and surface-tension dendrites oriented at 30° to one another. As can be seen from (2), the larger b along the channels favors greater velocity in these directions. The result is that for sufficiently large driving forces the kinetic term $\beta(\theta)v_n$ dominates the surface-tension anisotropy and stabilizes dendritic growth parallel to the channels. Note that the dominant effect here is not the directional variation of $\beta(\theta)$ but the prefactor of $b(\theta)^2$ in (2). On the other hand, by a simple energetics argument we can see that surface tension stabilizes dendrites at an angle of 30° to the channel grooves for velocities small enough for the surface-tension term to be dominant. For dendrites oriented in this direction the position of the interface is located where the effective distance between the plates is least. This minimizes the total surface area of the interface and the total energy necessary to stretch the interface into the dendritic shape, i.e., the increase in surface energy attendant to tip formation in a deep groove suppresses dendritic growth parallel to the grooves since this is the direction in which the interfacial area is maximized by the third dimension. These simple arguments based upon the interfacial boundary condition

match the experimental observation that near equilibrium surface tension is dominant, whereas further from equilibrium it is kinetic effects which stabilize the needle-crystal tip necessary for dendritic growth.

We emphasize that the shape of the morphologies which develop are sensitive to initial conditions. "Snowflakes" with 3, 6, or 12 branches are observed depending on the initial fastest-growing mode of the circle. As further support that kinetic dendrites are due to the anisotropy in b, in fourfold grooved cells the b^2 dependence of the interfacial velocity gives rise to slower dendrites growing at 45° to the main kinetic dendrites observed growing along the channels. Finally, in the absence of plate spacing ($b_0 = 0$) we are in the limit of zero surface tension (except within the channels). In this case, diffusion-limited-aggregation (DLA) structures are observed at low applied pressure, consistent with the notion that DLA is a zero effective surface-tension morphology, while at higher pressures dendritic-like or needle crystal-like structures appear depending on the channel widths.

MORPHOLOGY TRANSITIONS IN THE BOUNDARY-LAYER MODEL

Motivated by our Hele-Shaw results, we now draw upon the analogy established between the effects of anisotropy in interfacial pattern formation in the Hele-Shaw cell, computer simulations, analytic solutions of the full solidification problem,[10,13] and local models of solidification, and study the problem of the simultaneous effect of both surface-tension and kinetic anisotropies in the boundary-layer model for solidification. A true solution of the solidification problem requires solution of the diffusion equation $\partial T/\partial t = D\nabla^2 T$ with boundary conditions [e.g., Eqs. (3) and (4) below]. (D is the thermal diffusivity of the system.) Although much progress has been made over the past few years in solving this problem, it remains a serious computational problem. In particular, solution of the time-dependent problem for the advancing interface is very expensive computationally, and has only recently been successfully achieved.[12] It is for this reason that recent advances in the understanding of interfacial growth have frequently depended on local models. Thus, to date the BLM has proved a useful testbed to study the physics of diffusive growth. As a model of solidification it retains the interfacial diffusion of heat. Most critical to our study, the BLM is sufficiently tractable computationally to permit the study of both time-independent and time-dependent properties of the interface. As described below, this allows us to determine the evolved morphology starting from a wide range of hypothesized steady-state initial conditions. To date this has not been possible for the diffusion equation in solidification. Specifically, for the BLM we have been able to follow the time development in the three regimes found experimentally in anisotropic Hele Shaw: surface-tension anisotropy dominated dendritic growth, tip-splitting growth, and kinetic anisotropy dominated dendritic growth.

The key feature which emerges from our analysis is that the velocity dependence on driving force of dendrites

stabilized by surface tension is substantially different from that of dendrites stabilized by kinetic effects. This difference in scaling provides a qualitative explanation for morphology transitions which agrees with the Hele-Shaw morphology diagram, the results of our electrochemical deposition experiments, and previous experiments in crystallization from supersaturated solutions.[18] It further strongly suggests methods for more meaningful analysis of the results of growth in diffusion-controlled systems. Preliminary results from a solution of the full model of solidification for the selected needle-crystal velocities for either surface-tension anisotropy or kinetic anisotropy alone are consistent with this difference in scaling between selected velocities indicating that again the local BLM has captured the fundamental physics of morphology selection.

The boundary conditions for solidification are very similar to those for anisotropic Hele Shaw. Far from the growing solid the temperature of the supercooled melt is $T_\infty < T_M$ where T_M is the melting temperature of the solid. The velocity of interfacial advance is determined from the equation of continuity: the heat generated at the interface during solidification is the heat which diffuses into the melt. (In the one-sided model adopted here diffusion of heat in the solid is ignored.) With the material constants L, the latent heat of fusion, D, the thermal diffusion coefficient, C_p, the specific heat at constant pressure, and $\hat{n}$, the interface normal directed towards the melt, the normal velocity V_n of the interface satisfies:[19]

$$LV_n = -DC_p \nabla T \cdot \hat{n} . \tag{3}$$

The standard measure of the driving force of the system is the undercooling defined as $\Delta = (C_p/L)(T_M - T_\infty)$.

In the phenomenological treatment adopted here a form for the interfacial boundary condition, the Gibbs-Thomson temperature equivalent of Eq. (1), must be specified. In its simplest form the Gibbs-Thomson relationship for the interfacial temperature T_s is

$$T_s = T_M - \frac{L}{C_p} d_0 K , \tag{4}$$

where K is the curvature of the interface. Equation (4) results from arguments of macroscopic thermodynamics. On the basis of both microscopic considerations and experimental results we expect (4) to generalize to account for microscopic effects related to bonding anisotropy and the kinetics of atomic attachment. That the interfacial boundary condition should depend on kinetic effects has been experimentally demonstrated by Chan et al.[18] Their experiments on dendritic growth from supersaturated NH_4Cl solutions show a substantial variation of the tip velocity as a function of the system's supersaturation. These variations in velocity correspond to changes in the selected crystalline growth direction. This suggests that the general form of (4) should be

$$T_s = T_M - f(K, V_n) \tag{5}$$

and suggests the first-order expansion:

$$T_s = T_M - \frac{L}{C_p} d(\theta) K - \frac{L}{C_p} \beta(\theta) V_n . \tag{6}$$

Here θ is defined as the angle between the surface normal $\hat{n}$ and a fixed direction. Equation (6) must be considered only a first heuristic approximation to the interfacial boundary condition. Indeed it may be that the proper order of V_n should be less than or greater than unity. This may be the case in the Hele-Shaw cell[20] although here the physics does not translate to solidification. Generally, we believe that the function $f(K, V_n)$ must be a nonlinear function containing the activation effects which must exist to account for Chan et al.[18] observation. Nevertheless, whatever the "true" boundary condition may be, we believe that substantial insight can be gained by using (6) as a first approximation.

The specific functional forms of the surface-tension $d(\theta)$ and the kinetic coefficient $\beta(\theta)$ adopted below are

$$d(\theta) = d_0(1 - d_1 \cos m(\theta - \theta_d)) , \tag{7a}$$

$$\beta(\theta) = \beta_0(1 - \beta_1 \cos m(\theta - \theta_\beta)) . \tag{7b}$$

Here d_0 is the capillary length; the isotropic kinetic coefficient is β_0; d_1 and β_1 are dimensionless measures of the degree of the two anisotropies; m is the symmetry of the anisotropy; and, θ_d and θ_β are offset angles for surface-tension and kinetic effects, respectively. A dimensional analysis of β_0 suggests that it is useful to think of it as $d_0^{-1} \Omega^{-1}$ with Ω a characteristic frequency for kinetic attachment.

The inclusion of the offset angles θ_d and θ_β allows consideration of two possibilities: kinetic effects and surface tension can be aligned $(\theta_d = \theta_\beta)$ or they can be in competing directions $(\theta_d \neq \theta_\beta)$ as in the anisotropic Hele-Shaw cell. Since crystalline anisotropy is the microscopic source of both anisotropies it may be expected that surface-tension and kinetic anisotropy are aligned. On the other hand, the dependence of observed morphologies in Chan et al.[18] experiment on driving force (i.e., supersaturation) strongly suggests that as critical activation points are reached competitive effects arise which determine the morphology. While the offset angles θ_d and θ_β are at best a crude way to include such competitive effects, nevertheless doing so produces results in qualitative agreement with experimental observations. Moreover, the morphology diagram observed for the Hele-Shaw cell fits logically into the picture which emerges. It is with this physical motivation that we study the selected needle crystal velocities for both aligned and competing anisotropies.

The basic concept of the BLM is to assume that within a decay length l, the boundary layer, the temperature field at the interface relaxes to T_∞. This allows the BLM to capture most of the essential physics of the diffusion field, although it is not mathematically derivable from the diffusion equation for solidification. By contrast, if the diffusion equation were used the temperature field would decay only exponentially to T_∞. The BLM variable of interest is H, the heat content per unit interfacial length (or per unit area in three dimensions), defined as

$$H(S,t)=\int_0^\infty dz\, C_p[T(S,z)-T_\infty]\ ,\tag{8}$$

where the integration variable z is the distance away from the surface measured along the direction normal to the surface, and S is the arclength variable for the interface. An expression for the length l is obtained by assuming that $H=C_p(T_s-T_\infty)l$. In two dimensions the time evolution of the field H is given as the sum of the latent heat generated, the heat necessary to bring the portion of liquid which solidifies up to the temperature T_s from T_∞, the diffusion of heat along the interface, and a geometrical term resulting from the local change in arclength:[5]

$$\left.\frac{dH(S,t)}{dt}\right|_n=V_n[L-C_p(T_s-T_\infty)]$$
$$+DC_p\frac{\partial}{\partial S}\left[l\frac{\partial T_s}{\partial S}\right]-KV_nH\ .\tag{9}$$

Here S and t are the arc-length coordinate and the time, respectively. As time develops each interfacial point moves along the normal to the surface with velocity V_n. The notation $|_n$ refers to the fact that the derivative is evaluated using the infinitesimal difference dH as evaluated along this normal. This equation must be coupled with the equations describing the geometrical evolution of the interface. With $d\theta/dS=K$ it can be shown that

$$\frac{dS}{dt}=\int_0^S dS'K(S',t)V_n(S',t)\ ,\tag{10}$$

$$\left.\frac{dK[S(t),t]}{dt}\right|_n=-\left[\frac{\partial^2}{\partial S^2}+K^2\right]V_n\ .\tag{11}$$

These equations, coupled with the Eq. (8), completely define the time evolution of the interface and can be solved numerically.

Equations (9)–(11) may possess a steady-state solution, the needle crystal, which is expected to correspond closely to the dendritic solution. The velocity of this needle crystal can be determined via the "microscopic solvability criterion."[7,8] In the BLM the first step is to change reference frames to the moving frame of the presumed needle crystal. Assume that the needle-crystal tip is advancing with a constant velocity V_0. Directly from the definition of the normal velocity of the interface, it follows that if each point on the interface advances parallel to the direction of the tip with the velocity V_0 then $V_n(S)=V_0\cos\theta(S)$. Moreover, in the moving frame we have $\partial H(S,t)/\partial t=0$ and $\partial K(S,t)/\partial t=0$. Thus, using Eqs. (9) and (11), in the moving frame the needle crystal is defined by

$$V_n[L-C_p(T_s-T_\infty)]+DC_p\frac{\partial}{\partial S}\left[l\frac{\partial T_s}{\partial S}\right]$$
$$-KV_nH-\frac{\partial H}{\partial S}\frac{dS}{dt}=0\ ,\tag{12}$$

$$\frac{\partial K[S(t),t]}{\partial S}\frac{dS}{dt}+\left[\frac{\partial^2}{\partial S^2}+K^2\right]V_n=0\ .\tag{13}$$

Equation (13) with the moving frame expression for V_n

can be used to eliminate dS/dt from Eq. (10).

For the numerical computation scheme it is useful to introduce dimensionless fields as follows:[5]

$$h=\frac{\Delta^3H/L}{d_0},\quad \kappa=\frac{d_0K}{\Delta^3},\quad s=\frac{\Delta^3S}{d_0},\quad v_n=\frac{d_0V_n}{D\Delta^5}\ ,$$

and

$$u=\frac{C_p}{L}[T_s(S,t)-T_\infty]\ .$$

In terms of these fields Eq. (9) can be expressed as a system of three first-order coupled nonlinear differential equations:[7]

$$\frac{d\theta}{ds}=\frac{1}{\Delta^2 d(\theta)/d_0}\left[1-\frac{u}{\Delta}-\Delta^4\frac{D}{d_0}\beta(\theta)v_0\cos\theta\right]$$
$$=\kappa\ ,\tag{14}$$

$$\frac{du}{ds}=\lambda\ ,\tag{15}$$

$$\frac{d\lambda}{ds}=2\Delta^2\lambda v_0\sin\theta+\Delta^2 v_0\kappa u\sec\theta$$
$$-\Delta^4 v_0^2\cos^2\theta\frac{1-u}{u}-\frac{\lambda^2}{u}-\lambda\kappa\tan\theta\ .\tag{16}$$

With boundary conditions, Eqs. (14), (15), and (16) define a nonlinear eigenvalue problem for the selected velocity of the needle crystal.[7] The problem is posed in terms of the value of the so-called "mismatch function" $\lambda(s=0,v_0)$. For a needle-crystal solution to these equations to exist u, the dimensionless temperature at the surface, must be symmetric about the origin. This requires that $\lambda(s=0,v_0)=0$. For given parameters (i.e., Δ, m, d_0, d_1, β_0, and β_1) the eigenvalue v_0 is determined by integrating the equations from the initial conditions at $\theta=\pi/2$ (i.e., $s\to\infty$) back to $\theta=0$ (i.e., $s=0$) for a trial v_0. If the mismatch function vanishes then the velocity eigenvalue, the selected velocity v^*, has been found. As a practical numerical matter, the mismatch function never completely vanishes. However, one can integrate the equations from the initial conditions to $s=0$ ("shoot backwards") and find the range of v_0 over which $\lambda(s=0,v_0)$ changes sign. The selected velocity eigenvalue v^* is then determined by interpolation. It is also possible for there to be more than one value of v_0 such that $\lambda(s=0,v_0)=0$. In this case it is the largest v_0 determined which corresponds to v^*.[5] This method of determining v^* constitutes the microscopic solvability condition as applied to the BLM.

It remains to specify the boundary conditions for these equations. This is accomplished by observing that Eqs. (14)–(16) possess fixed points at $\theta=\pm\pi/2$ (i.e., $s=\pm\infty$). It can be shown[5] that there is only one trajectory leading into these fixed points, and that this trajectory is asymptotically identical to the equivalent Ivantsov trajectory. (Recall that the Ivantsov solution is a needle crystal in the absence of either surface-tension or kinetic effects.[19]) Since at $\theta=\pm\pi/2$ the needle crystal is expected to have vanishing curvature and normal velocity, the Ivantsov solution *with the specified needle-crystal velocity* is asymp-

totically a better and better approximation to the needle-crystal solution. This provides initial conditions at $\theta=\pi/2$ of $\kappa(\pi/2)=0$ and $\lambda(\pi/2)=0$, i.e., the Ivantsov conditions at $\theta=\pm\pi/2$.

An additional question arises when solving for the selected velocity in the case of competing anisotropies. Competing anisotropies mean that θ_d and θ_β are unequal. This leaves undetermined the direction of the steady-state solution for the needle-crystal tip. On physical grounds, and justified by our simulations, we choose one of the two offset angles to be zero. This is tantamount to assuming that the needle crystal is stabilized either by surface tension anisotropy ($\theta_d=0$) or by kinetic anisotropy ($\theta_\beta=0$), and is not oriented somewhere in between. Needle crystals stabilized in the former fashion we designate as *surface-tension needle crystals*, those stabilized in the latter manner are *kinetic needle crystals*. A study of the effects of competition between the two anisotropies now requires computation for given Δ of selected velocities for both orientations, i.e., both $\theta_d=0$ and $\theta_\beta=0$.

To develop a quantitative and qualitative understanding of the relative importance of surface tension and kinetic anisotropy on morphology selection, we now proceed to evaluate numerically the selected velocity for a range of parameters d_0, d_1, β_0, and β_1.

In Fig. 3 selected velocities as a function of undercooling Δ are plotted for the case of six-fold symmetry and a range of surface-tension and kinetic parameters. Kinetic anisotropy and surface tension anisotropy are alternately neglected in Figs. 3(a) and 3(b). The units of V^*, the selected velocity, are d_0/D (i.e., $V^*=v^*\Delta^5$). It is known[13] that in the limit of vanishing Péclet number ($\Delta\rightarrow0$) the selected velocity $V^*\sim\Delta^4$. However, the log-log presentation of the higher undercooling regime studied here shows that surface-tension anisotropy and kinetic anisotropy give rise to V^* scaling with Δ with a rough difference in exponents of ≈3. The parameter regime chosen is such that there is a significant overlap in V^* between the two cases. For surface-tension and kinetic term parameters of comparable strength, comparison of Figs. 3(a) and 3(b) shows that surface-tension anisotropy selects larger V^* than kinetic anisotropy at low undercooling, while the larger exponent for kinetic anisotropy determined V^* results in this reversing at larger Δ. Thus, in systems where both surface-tension and kinetic effects are of the same order of magnitude, at low driving force surface-tension anisotropy will be dominant in determining the selected velocity, whereas at high driving force V^* will be predominantly determined by kinetic effects. For intermediate driving forces whether the two anisotropies are aligned or competing will be critical to the value of V^* and the selected morphology. This scenario corresponds precisely to our anisotropic Hele-Shaw observations. Moreover, the conclusions drawn above from the local BLM are now supported by preliminary work solving the full diffusion problem. Our initial numeric studies of the dependence of V^* shows roughly the same difference in scaling as a function of undercooling between surface-tension and kinetic anisotropies. For this reason, we expect that the analogues of Figs. 3, 4, and 5 will be obtained for the full diffusion equation.

In Fig. 4 are provided two representative plots of selected velocities for the case of aligned surface-tension and kinetic anisotropies. The primary observation is that these log-log plots display no linear region: when kinetic and surface-tension effects combine the result is v^* does not scale with Δ as it would for either anisotropy alone. This may be experimentally observable. Our computations were limited in accuracy at about $\Delta=0.2$. Presumably in experiments with greater range, or where the on-
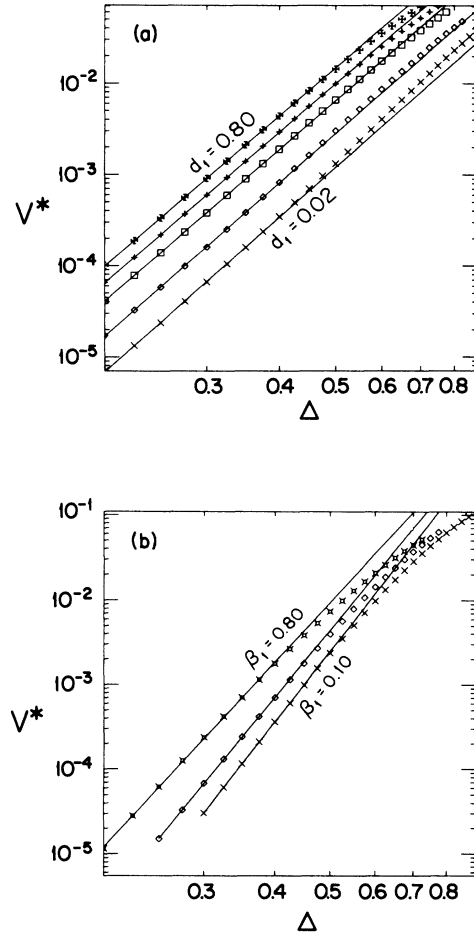

FIG. 3. Log-log plots of the selected velocity V^* as a function of the undercooling Δ in the BLM for different values of the anisotropy. Here V^* is measured in units of D/d_0. The straight lines through the computed values of V^* are least-square fits. The fits were done over the range $0.2<\Delta<0.4$. (a) Surface-tension anisotropy selected velocities computed for different values of d_1 ($d_0=1.0$, $\beta_0=1.0$, $\beta_1=0$). Beginning with the lowermost set of data points the values of d_1 are 0.02, 0.06, 0.20, 0.40, and 0.80. The bracketing values of the best fits are for $d_1=0.02$, $V^*\sim\Delta^{5.64}$ and for $d_1=0.80$, $V^*\sim\Delta^{5.47}$. (b) Kinetic anisotropy selected velocities computed for different values of β_1 ($d_0=1.0$, $d_1=0.0$, $\beta_0=1.0$). Beginning with the lowermost set of data points the values of β_1 are 0.10, 0.20, and 0.80. The bracketing values of the best fits are for $\beta_1=0.10$, $V^*\sim\Delta^{8.61}$ and for $\beta_1=0.80$, $V^*\sim\Delta^{7.26}$. Throughout the assumed symmetry was $m=6$. Computations were done with $d(\theta)=d_0[1.0-d_1\cos(m\theta)]/(d_0+d_1)$.
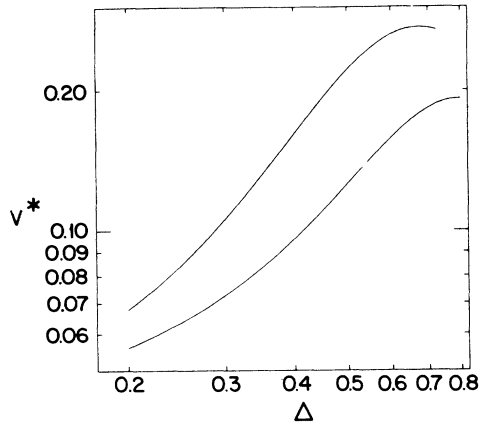
FIG. 4. Log-log plots of the selected velocity v^* for aligned surface-tension and kinetic anisotropies. Here v^* is measured in units of $D\Delta^5/d_0$. Scaling out the undercooling enhances the transition from surface-tension to kinetic term dominated needle-crystal growth. The lower curve is for $d_1=0.06$, $\beta_0=1.0$, and $\beta_1=0.06$. The upper curve is for $d_1=0.06$, $\beta_0=1.0$, and $\beta_1=0.40$. $m=6$ in both cases. Computations were done with $d(\theta)=d_0[1.0-d_1\cos m(\theta)]/(d_0+d_1)$.

set of kinetic effects is more sudden (perhaps due to activation), a change in the observed power-law behavior would be the signature of the onset of kinetic effects.

We now proceed to consider the effect of competition of anisotropies when the surface-tension and kinetic anisotropies are offset by 30° and the anisotropy is again assumed to be sixfold ($m=6$). Crossing of the curves for the selected velocities for either surface-tension or kinetic effects alone is used to judge that the two anisotropies are
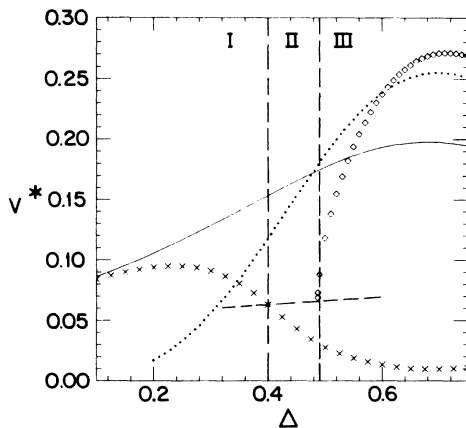

FIG. 5. The selected velocity v^* for $d_0=\beta_0=1.0$ and competing anisotropies. v^* is measured in units of $D\Delta^5/d_0$. ———, surface-tension anisotropy ($\beta_1=0$, $d_1=0.15$); $\cdots$, kinetic anisotropy ($d_1=0$, $\beta_1=0.40$); and for $d_1=0.15$, $\beta_1=0.40$: $\times$, v^* surface-tension needle crystals ($\theta_d=0$, $\theta_\beta=0.5236$); $\lozenge$, v^* for kinetic needle crystals ($\theta_d=0.5236$, $\theta_\beta=0$); — — —, possible v^* behavior for tip-splitting DBM growth between surface-tension and kinetic anisotropy regimes. Computations were done with $d(\theta)=d_0[1.0-d_1\cos(m\theta)]/(d_0+d_1)$ and with $m=6$.

of comparable strengths. In Fig. 5 the result of their competition is indicated by dividing the plot of v^* into three regions of selected morphologies as a function of the undercooling Δ. In region I surface tension is dominant, and the needle crystal corresponding to the selected velocity is stable. This is concluded from the simulation of the time development of the surface-tension dendrite as shown in Fig. 6(a). In region III kinetic effects are dominant, the selected needle crystal is stable, and the kinetic dendrite of Fig. 6(c) emerges during time develop-
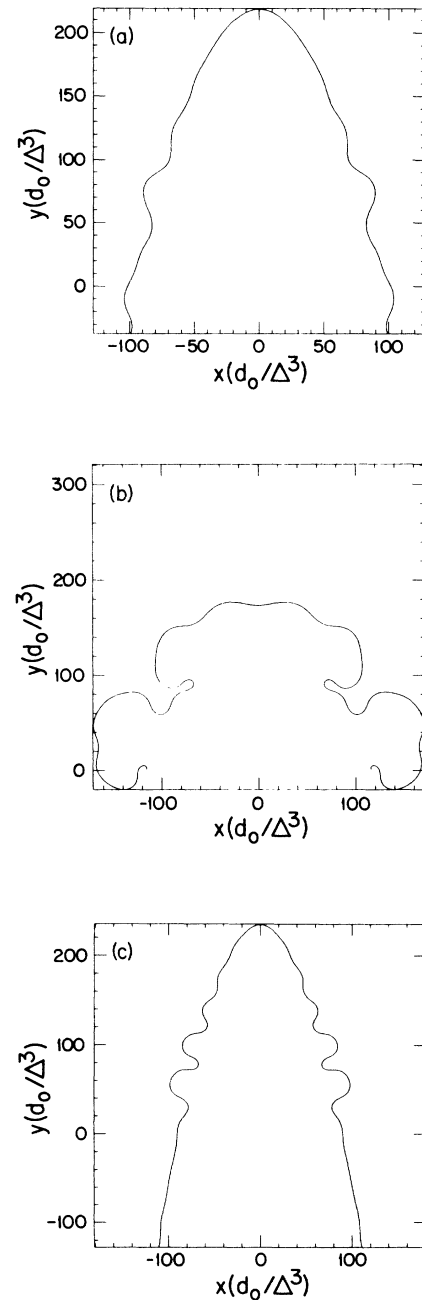

FIG. 6. (a) Surface-tension dendrite ($\Delta=0.375$, $t=3000$); (b) tip-splitting growth ($\Delta=0.475$, $t=4500$); (c) kinetic dendrite ($\Delta=0.50$, $t=2000$). Arclength is measured in units of d_0/Δ^3 and time t in units of $d_0^2/D\Delta^5$.

ment of the needle crystal. Region II, however, corresponds to the development of an effective "gap" in the selected velocity. Near $\Delta \approx 0.46$ the two competing anisotropies are closest in effective strength. The result is a dramatic decline in the selected velocity for either surface-tension or kinetic needle crystals. Moreover, Fig. 6(b) shows that for these undercoolings there is no stable needle-crystal growth.

To close the gap of region II we assume that the selected morphology for this range of undercooling is that of the DBM, i.e., the tip-splitting morphology which corresponds most closely to the unstable growth shown in Fig. 6(c). With this in mind, we have sketched in a possible plot of the selected velocity for the DBM through the region of unstable needle-crystal growth. This sketch is of course very speculative. The monotonic increase in velocity shown for the DBM is physically motivated by the increasing driving force provided by the undercooling. On the other hand, at this writing it is unknown how to compute the DBM velocity, or how to define it. Presumably prior to tip splitting a branch may have a well-defined velocity; however, during the tip-splitting event simulations indicate that there is a slowing of the tip. Despite all these difficulties, it seems sensible to us that some working definition for the velocity of the DBM can be arrived at, and that the one sketched here makes physical sense.

Two prominent features of Fig. 5 are (i) there is a critical undercooling Δ_c, below which there is no selected velocity for a kinetic needle crystal, and (ii) there is a range of undercoolings in which there is a selected velocity for both surface-tension and kinetic needle crystals. With respect to (i), it is important to emphasize that it is not that the kinetic needle crystal is unstable for $\Delta < \Delta_c$, or that the selected velocity goes to zero near Δ_c. As discussed above, for a needle crystal to exist the mismatch function must vanish for a selected velocity. Figure 7 is a plot of the mismatch function $\lambda(s = 0, v_0)$ near $\Delta_c = 0.487$ for the parameters of Fig. 5. It is evident that the mismatch function fails to vanish at Δ_c. As a result, if kinetic dendrites are the selected morphology for $\Delta > \Delta_c$, a plot of morphology velocity versus Δ will very likely either have a jump discontinuity, or at least a discontinu-
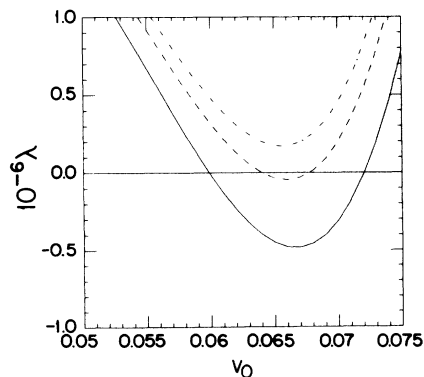
ous derivative when the transition to kinetic dendritic growth occurs. By contrast, observation (ii) is that for surface-tension needle-crystal growth the mismatch function does vanish over the entire range of undercoolings studied. However, as indicated by Fig. 6(b), the surface-tension needle crystal is unstable and tip splits beyond region I of Fig. 5. In particular, for the undercoolings for which there is a selected needle crystal due to either surface-tension or kinetic effects time-dependent studies show that the slower needle crystal (i.e., the surface-tension needle crystal) is unstable and tip splits.

It is these observations which give rise to our hypothesis that the selected morphology of the system is the fastest growing one. This is analogous to the observation that when the mismatch function has multiple zeros, i.e., several "selected" velocities, the only stable dendrite is the one with the largest velocity. Our first example of the fastest growing morphology principle are the kinetic dendrites in the BLM: the needle crystal for surface-tension dendrites at the same undercooling is found to be unstable against tip splitting. Our hypothesis is that for parameters corresponding to region III of Fig. 5 only the dendritic growth would be observed, as opposed to the presence of a combination of kinetic dendritic growth with tip-splitting growth on other branches arising from unstable surface-tension growth. In a like manner, in the region II gap of Fig. 5 the sketched DBM velocity is greater than the selected velocity for the surface-tension needle crystals (which are indeed unstable). If we could compute the DBM velocity we might find that it too continues to increase through the kinetic dendrite morphology regime, but having the smaller velocity it would not be the selected growth. Again, our principle of the fastest growing morphology is that within the gap only DBM growth is observed. This growth is not intermixed with "failed" surface tension dendrites. And within region III only kinetic dendrites are observable; although there may be a computable velocity for DBM growth in this regime it will not emerge in the experimental context. Despite our expectation of the rule of the fastest growing morphology, for parameters near the transition between regions experimental fluctuations in the local environment will give rise to the simultaneous appearance of two morphologies.

The behavior of the selected morphology as a function of velocity as shown in Fig. 5 combined with the fastest growing morphology hypothesis outlined above leads us to an analogy between phase transitions[21] and morphology transitions. Using the hypothesized behavior of the DBM selected velocity shown, the transition from surface-tension dendrites to DBM growth is analogous to a second-order phase transition: the selected velocity is continuous as a function of undercooling, but shows a discontinuity in its slope. In keeping with this analogy, the transition from DBM growth to kinetic dendrites is first order with the jump in v^*. As indicated above, this transition should be at least a second-order-like since the kinetic mismatch function fails to vanish at the reentrant transition from tip splitting to dendritic growth and it is unlikely that the selected DBM velocity curve will have the matching slope at this point. From Fig. 5 we can also

FIG. 7. Mismatch function λ vs v for $\theta_d = 0.5236$, $d_1 = 0.15$, and $\beta_1 = 0.40$: (———), $\Delta = 0.4874$; (— — —), $\Delta = 0.4872$; and —·—·—·, $\Delta = 0.4871$.

logically conclude, and our numerical studies support, that by varying the microscopic control parameters a wide range of scenarios of morphology transitions can be produced. In our example we find surface tension dendrites, DBM, and kinetic dendrites with increasing undercooling. With different microscopic parameters it is possible for there to be no intermediate DBM morphology and the transition between surface-tension and kinetic dendrites with competing anisotropies can be first- or second-order-like; or, for sufficiently weak surface-tension anisotropy there may be no regime of surface-tension dendrites but only a direct transition from DBM growth to kinetic dendrites. Finally, in three dimensions first- or second-order-like transitions between different crystallographic symmetries of kinetic dendrite growth are also possible.

QUALITATIVE COMPARISON
BETWEEN THEORY AND EXPERIMENTS

The qualitative analogy between the computed morphology transitions in the boundary-layer model and the Hele-Shaw experiments reported in the earlier section are self-evident. In both cases the competition between surface-tension anisotropy and kinetic anisotropy gives rise to surface-tension dendrites, tip-splitting growth, and then kinetic dendrites as the driving force is increased. More direct comparison to solidification experiments is unfortunately not possible for two reasons. First, solidification experiments for the higher undercoolings of our computations have not been performed. Second, the boundary-layer model for solidification may never have a direct experimental realization: as discussed above, as a local model it incorporates the physics of the diffusion field, but may not translate directly to real experiments. As a result, the primary profit to be had from the BLM analysis is to recognize the correlation between microscopic effects, morphology transitions, and how these manifest themselves in the velocity of the interface, this latter being an experimentally accessible number. In particular, the experimental data of Chan et al.[18] for the velocity of growth of dendrites from supersaturated NH_4Cl solution fits well in the framework of morphology transitions defined above. In their experiments they found that corresponding to changes in crystallographic orientation of the dendrite there was either a jump discontinuity or a discontinuity in the slope in the plot of observed dendritic velocity versus supersaturation. Thus, in our morphology transition nomenclature, we would identify their observed transition from $\langle 100 \rangle$ to $\langle 110 \rangle$ dendritic growth as a second-order morphology transition (change in slope), while their transition from $\langle 110 \rangle$ to $\langle 111 \rangle$ growth is a first-order morphology transition (a jump discontinuity).

Experiments in growth by electrochemical deposition (ECD) also produce results in qualitative agreement with the characterization of morphology transitions advanced here. Sawada et al.[2] have plotted the interfacial velocity versus applied voltage. A comparison between their morphology diagram and plotted velocities indicates that in their experiments sudden changes in slope of v versus V

correspond to morphology transitions. In our own experiments of electrodeposition of Cu from $CuSO_4$ we have observed changes in interfacial velocity corresponding to a change in microstructure.[22] We are not suggesting that these morphology transitions are necessarily due to competition between surface-tension and kinetic anisotropies as in the Hele-Shaw experiment or the BLM. The three-dimensional nature of the growth adds a great variety of competing effects to the problem. Just as in the Chan et al. experiment, in ECD we expect competition between different crystallographic directions both in surface-tension and kinetic attachment. These effects are not accounted for in the BLM with the boundary conditions used here. Nevertheless, as in the case of the BLM and the Hele-Shaw cell, some of the morphology transitions in ECD can be put into correspondence with changes in slope in the interfacial velocity versus driving force plot. This again demonstrates the utility of this characterization of morphology transitions.

CONCLUSIONS

In the above we have combined experimental and theoretical observations as a first step towards a coherent picture of the underlying physics of interfacial pattern formation in diffusion-controlled systems. Using the anisotropic Hele-Shaw cell we have provided experimental realization of surface-tension and kinetic dendrites. We generalized the insights gained from this system by solving a theoretical model for diffusion-controlled growth, the boundary-layer model, for corresponding conditions. Within the BLM we showed that tip-splitting growth may arise as a result of competition between surface-tension and kinetic anisotropies. More dramatically, we found that in the BLM morphology transitions may be either continuous or discontinuous as characterized by the selected needle-crystal velocity. This follows from plots of the interfacial velocity versus the driving force (i.e., the undercooling). With this organization in mind we found that in the BLM morphology transitions, by analogy to phase transitions, may be either first- or second-order-like depending upon whether the selected velocity was discontinuous or showed a sudden change in slope at the undercooling for which the morphology transition was observed. Following from these plots of the selected velocity is our hypothesis that it is the fastest growing morphology which is selected. Although we do not know at this time how to compute the interfacial velocity of the dense-branching morphology, we deduce from our BLM time-dependent simulations, and the results of our experiments, that the selected velocity of the DBM is greater than that of a dendritic needle crystal in the parameter range of its observation.

Many questions remain unanswered. First, we still lack a fundamental understanding of the tip-splitting instability. Our time-dependent simulations indicate that it is nonlinear in nature. The outstanding questions are how to go beyond linear stability analysis to determine the parameter range of tip-splitting growth, and the concurrent problem of a selection principle for the velocity of the dense-branching morphology. The second ques-

tion to be addressed is whether the solution for the selected needle-crystal velocity for the full diffusion equation gives results comparable to that of the BLM. Our preliminary answer is yes, although at this time the matter of scaling exponents with undercooling and the effect of competition is a matter under investigation. More direct comparison to experiment will also require a generalization of the competition model presented here. In real physical systems it is to be expected that the competition may arise due to a competition of crystallographic symmetries. In addition, in three dimensions the morphology space must be much richer than that of two dimensions: the crystallographic symmetries of three dimensions are simply greater than that of two dimensions. Of course it is not only the geometry of our theoretical model which must be improved. The competition as expressed in the boundary conditions of our BLM model lacks the physics of activation which a more realistic model must include. It is at this level, the level of modeling the microscopic dynamics, that the most research is required. Throughout our presentation kinetic effects have been emphasized. On the basis of the Hele-Shaw experiments, and other experimental observations, as well as the heuristic of the BLM results, they must play an important role in morphology selection. On the other hand, to date there are no experimental measurements of kinetic parameters. It is the quantification of such physical effects which must be achieved in order to be able to understand and control morphology selection and transitions.

ACKNOWLEDGMENTS

[1]E. Ben-Jacob, R. Godbey, N. D. Goldenfeld, J. Koplik, H. Levine, T. Mueller, and L. M. Sander, Phys. Rev. Lett. **55**, 1315 (1985).

[2]Y. Sawada, A. Dougherty, and J. P. Gollub, Phys. Rev. Lett. **56**, 1260 (1986).

[3]D. Grier, E. Ben-Jacob, R. Clarke, and L. M. Sander, Phys. Rev. Lett. **56**, 1264 (1986).

[4]V. Horvath, T. Vicsek, and J. Kertesz, Phys. Rev. A **35**, 2353 (1987).

[5]E. Ben-Jacob, N. D. Goldenfeld, J. S. Langer, and G. Schön, Phys. Rev. Lett. **51**, 1930 (1983); Phys. Rev. A **29**, 330 (1984).

[6]R. Brower, D. A. Kessler, J. Koplik, and H. Levine, Phys. Rev. Lett. **51**, 1111 (1983).

[7]E. Ben-Jacob, N. D. Goldenfeld, B. G. Kotliar, and J. S. Langer, Phys. Rev. Lett. **53**, 2110 (1984).

[8]D. A. Kessler, J. Koplik, and H. Levine, Phys. Rev. A **30**, 3161 (1984).

[9]E. Ben-Jacob, G. Deutscher, P. Garik, N. D. Goldenfeld, and Y. Lareah, Phys. Rev. Lett. **57**, 1903 (1986).

[10]D. A. Kessler and H. Levine, Phys. Rev. A **33**, 7867 (1986).

[11]D. I. Meiron, Phys. Rev. A **33**, 2704 (1986).

[12]Y. Saito, G. Goldbeck-Wood, and H. Müller-Krumbhaar, Phys. Rev. Lett. **58**, 1541 (1987).

[13]J. S. Langer, in *Chance and Matter*, 1986 Les Houches Lectures, Session XLVI, edited by J. Souletie, J. Vannimenus, and R. Stora (North-Holland, Amsterdam, 1987).

[14]L. Paterson, J. Fluid Mech. **113**, 513 (1981).

[15]A. Buka, J. Kertesz, and T. Vicsek, Nature **323**, 424 (1986).

[16]S. N. Rauseo, P. D. Barnes, and J. V. Maher, Phys. Rev. A **35**, 1245 (1987).

[17]G. Daccord, J. Nittmann, and H. E. Stanley, Phys. Rev. Lett. **56**, 336 (1986).

[18]S.-K. Chan, H.-H. Reimer, and M. Kahlweit, J. Cryst. Growth. **32**, 303 (1976).

[19]J. S. Langer, Rev. Mod. Phys. **52**, 1 (1980).

[20]C.-W. Park and G. M. Homsy, J. Fluid Mech. **139**, 291 (1984).

[21]L. D. Landau and E. M. Lifshitz, *Statistical Physics*, 2nd ed. (Addison-Wesley, Reading, MA, 1969).

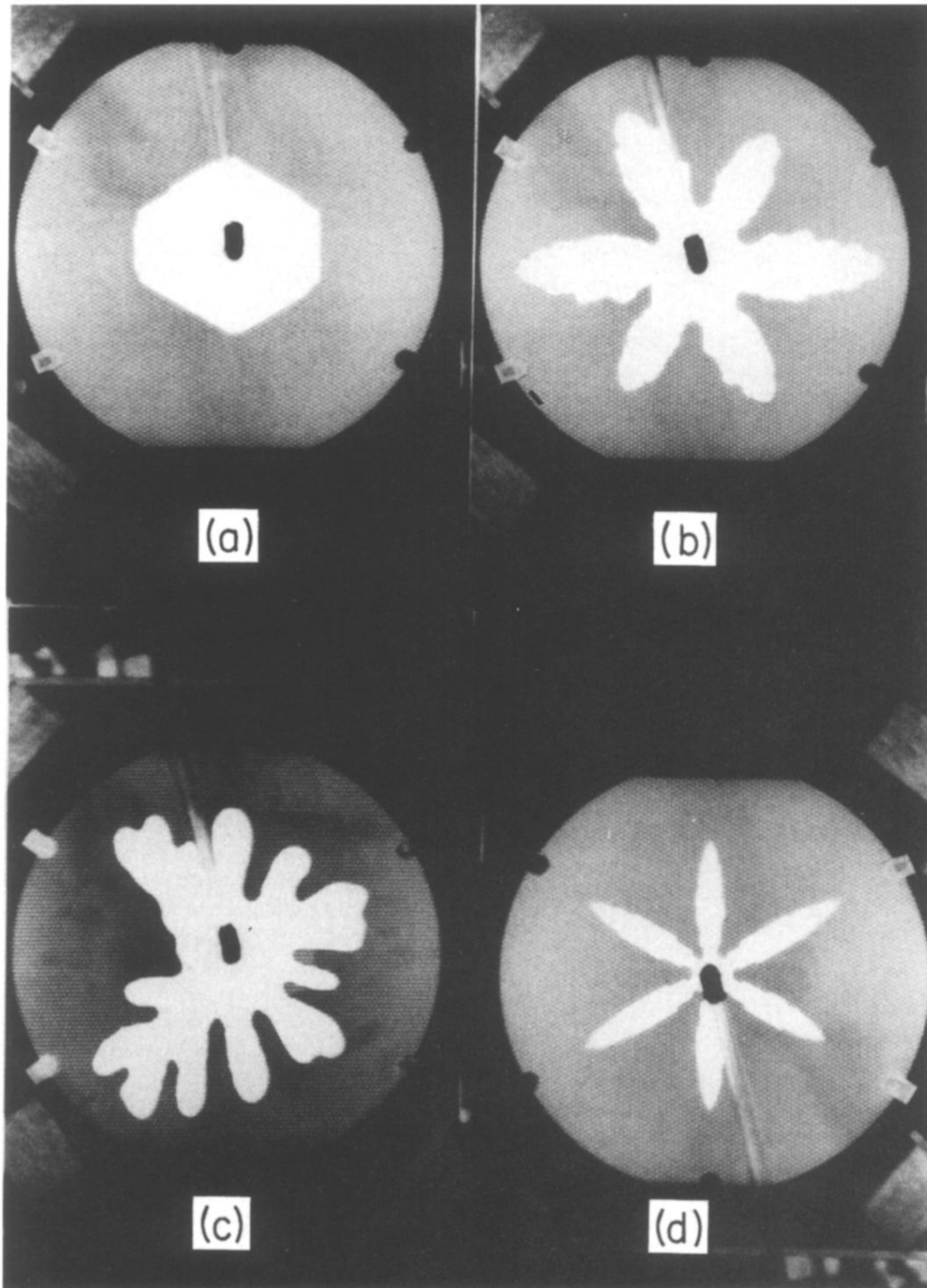[22]E. Ben-Jacob, N. Broxholm, P. Garik, and B. Orr (unpublished).

FIG. 2. Morphologies corresponding to the morphology diagram in the anisotropic Hele-Shaw cell. (a) Faceted growth. (b) Surface-tension dendrites. With careful inspection it is possible to observe that the dendrite tips are pointed at an angle of 30° to the ruling of the grooves. (c) Tip-splitting growth. In a larger and more regular cell we assume that this would be a dense-branching growth. (d) Kinetic dendrites. The needle crystals grow parallel to the ruled channels.